ACS Macro Letters

Letter

pubs.acs.org/macroletters

# Fractionated Crystallization of Defect-Free Poly(3-hexylthiophene)

P. Kohn,[†] S. Huettner,[†] U. Steiner,[†] and M. Sommer*[,‡,§]

[†]Cavendish Laboratory, Department of Physics, University of Cambridge, J J Thomson Avenue, Cambridge CB3 0HE, United Kingdom

[‡]Melville Laboratory for Polymer Synthesis, University of Cambridge, Lensfield Road, Cambridge CB2 1EW, United Kingdom

Supporting Information

**ABSTRACT:** Fractionated crystallization (FC), a chain-sorting mechanism by length, is identified in well-defined, low molecular weight, and defect-free regioregular poly(3-hexylthiophene) by X-ray scattering and calorimetry of bulk samples. While wide-angle X-ray scattering (WAXS) qualitatively suggests that the degree of crystallinity is similar in all investigated samples, the melting enthalpies are largely different. We ascribe this to intricacies in the integration of the melting and crystallization peaks in calorimetric experiments, which is caused by FC occurring over a large temperature range. The extent of FC decreases with increasing molecular weight and increases with increasing polydispersity. The temperature-dependent investigation of the long period $L_P$ and the (100)-WAXS reflection of a sample in which FC is absent allows to disentangle effects from main-chain and side-chain crystallization.

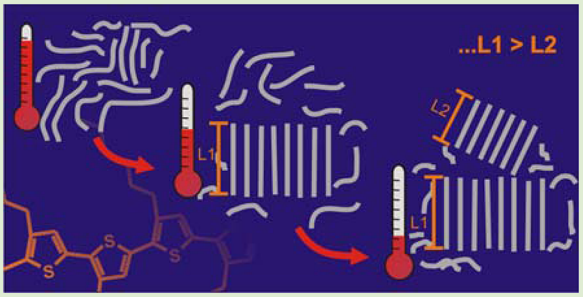


Crystallization in semicrystalline polymers commonly occurs by nucleation and growth of stacks of lamellae, giving rise to spherulites if the nucleation density is small enough. Two different kinds of grain boundaries (GBs) are distinguished: (i) GBs arising from the interlamellar amorphous phase and (ii) GBs between different spherulites or stacks of lamellae nucleated at different points.[1] In semicrystalline conjugated polymers, a detailed knowledge of morphology is key to controlling all opto-electronic properties, including bulk charge transport.[2,3] Regioregular poly(3-hexylthiophene) (rrP3HT) is an archetype semicrystalline conjugated polymer that is often used in organic electronic devices.[4−7] Unlike polyethylene (PE), the observation of spherulites in films of rrP3HT requires slow crystallization from a solvent vapor swollen sample to achieve sufficiently low nucleation densities.[8] A further difference between the well-studied PE and rrP3HT is the relatively low degree of polymerization (DP) of rrP3HT, which is often below 100. Hence, these materials are probably better compared to *n*-alkanes than to polyethylene.[9] Mixtures of different monodisperse *n*-alkanes with $n \sim 30$ show fractionated crystallization (FC), that is, sorting of chains by their length.[10,11] On the other hand, Zeng et al. have reported that mixtures of longer *n*-alkanes are less prone to fractionate.[12] As FC provides a mechanism by which chains of different lengths can efficiently crystallize, such a process should lead to an increased number of spherulitic boundaries or boundaries between different stacks. As a result, the degree of crystallinity should be unaffected or even enhanced. Through FC in low molecular weight rrP3HT, the shorter chains might be able to crystallize, which will influence the nature of intercrystalline material, number of grain boundaries, and the degree of crystallinity and, hence, will be important for bulk and thin film charge transport. Generally, the charge carrier mobility of poly(3-alkylthiophene)s is reduced within amorphous regions compared to crystalline ones.[13,14] Another often observed trend is the apparent molecular weight (MW) dependence of charge mobility in organic thin film transistor (OFET) devices, which usually leads to differences in mobility by several orders of magnitude.[15−18] This dependence has been attributed to several factors, such as the domain boundary structure, inherent effects of chain length,[15,18] degree of crystallinity,[19] or backbone conformation.[20] The picture of enhanced electrical interconnection of crystallites in high molecular weight P3HT films invokes the existence of so-called "tie-molecules" that span across amorphous layers,[13,14,18] which obviously are more likely for higher MWs.[21,22] Crossland et al. have recently highlighted that the number of spherulitic boundaries across an OFET-channel in solvent vapor-annealed P3HT films considerably influences charge carrier mobility.[23] Contrasting these findings from OFET experiments, Goh et al. found a less significant behavior in diode configurations,[24] whereas Ballantyne et al. carried out time-of-flight experiments and reported a reversed dependence of mobility on MW.[25] Recently, Neher et al. distinguished between local and macroscopic transport in thin films of different molecular weight and concluded that while intracrystalline transport is relatively unaffected by molecular weight, macroscopic transport in low molecular weight films is severely hampered by disordered domains.[26] These discrepancies of experimental results highlight the still existing difficulty in establishing structure−function relationships,

**Received:** July 23, 2012
**Accepted:** September 14, 2012
**Published:** September 18, 2012

   dx.doi.org/10.1021/mz3003769 | *ACS Macro Lett.* 2012, 1, 1170−1175

**Table 1. Physical and Thermal Properties of As-Synthesized Samples 1−3[a]**

| sample | $M_{n,MALDI}$ (g/mol) | $PDI_{MALDI}$ | $DP_{MALDI}$ | $l_c$ (nm) | $M_{n,GPC}$ (g/mol) | $PDI_{GPC}$ | $T_m$ (°C) | $T_c$ (°C) | $\Delta H_m$ (J/g) | $\Delta H_c$ (J/g) | $L_P$ (nm) |
|---|---|---|---|---|---|---|---|---|---|---|---|
| **1** | 2942 | 1.042 | 18 | 6.5 | 4000 | 1.15 | 152.7 | 139.3 | 10.1 | 10.2 | 8.5 |
| **2** | 3709 | 1.032 | 22 | 8.2 | 5400 | 1.13 | 179.9 | 164.5 | 21.8 | 22.5 | 9.8 |
| **3** | 3480 | 1.051 | 21 | 7.7 | 6300 | 1.15 | 179.3 | 165.7 | 16.6 | 15.3 | 9.8 |
| **3a** | 4036 | 1.014 | 24 | 8.8 | 7900 | 1.06 | 190.5 | 177.1 | 30.5 | 29.2 | 9.6 |
| **3b** | 3384 | 1.025 | 20 | 7.3 | 5900 | 1.06 | 165.9 | 155.4 | 17.4 | 16.2 | 8.4 |

[a] **3a** and **3b** were obtained from **3** via preparative GPC. $l_c = (DP - 1)/0.383$ nm. The thermal properties are determined by DSC from the first cooling and second heating cycle at 10 K/min.

which may partly reflect the lack of understanding structure formation in such complex materials.

Recently, we have shown that rrP3HT prepared by Kumada Catalyst Transfer Polymerization (KCTP) using $NidpppCl_2$ as the catalyst[27,28] contains one single tail-to-tail (TT) defect which is distributed over the otherwise fully regioregular chain, and that defect-free P3HT (dfP3HT) can be obtained via externally initiated KCTP.[29] The comparison of rrP3HT with dfP3HT showed that partial inclusion of TT defects into the crystal occurs.[29] These new possibilities of refined synthesis now open up further crystallization studies, as the entire chain of dfP3HT is crystallizable. This is especially interesting for low molecular weights forming chain-extended crystals that allow for the observation of side-chain crystallization[30] and a long period $L_P$.[17,29,30]

Here we identify fractionated crystallization (FC) as a function of the degree of polymerization (DP) and polydispersity index (PDI) in a series of well-defined, low molecular weight dfP3HT as a potential source of additional grain boundary formation. Three samples with varying molecular weight dfP3HT **1**−**3** were prepared via external initiation of KCTP.[29] To further reduce the obtained low PDI of 1.15−1.13, sample **3** was fractionated using preparative GPC to give **3a** and **3b**. The obtained set of materials had DP = 18−24 and PDIs = 1.05−1.15, as determined by MALDI-ToF and GPC, respectively (Table 1, Figure S1). The very low PDIs obtained from MALDI-ToF are likely underestimated.[29] GPC does not provide absolute molecular weights, but the data is included for comparison with the literature. In a previous paper, we used $^1$H NMR for the determination of the DP in the range DP = 40−80,[29] but in the case of the small DP ∼ 20 used here, MALDI-ToF gave the most accurate results. Figure 1 shows the chain length distribution $p(N)$ as a function of the DP determined by MALDI-ToF. The low PDI of samples obtained by preparative GPC is clearly visible (Figure 1, Table 1).

Figure 2a shows a schematic of the semicrystalline structure of P3HT and Figure 2b the combined small angle (SAXS) and wide-angle X-ray (WAXS) scattering pattern of **3a** after cooling from the melt at 10 K/min. The microstructure is characterized by alternating amorphous and crystalline domains, which give rise to the long period $L_P$ (Figure 2b). The crystalline domains consist of another layered structure defined by the main chain−side chain separation ($a$-axis). The $\pi-\pi$ stacking of the planarized backbones is along the $b$-axis, and the $c$-axis points along the polymer backbone. Because the SAXS $L_P$ peaks are more pronounced for small DPs, samples with DPs between 18 and 24 are used here. Sample **3a** with a DP of 24 and a PDI of 1.06 shows a sharp $L_P$ peak with second and third order reflections, which demonstrates the usefulness of defect-free and low molecular weight materials with very low polydispersity for the present study (Figure 2b).

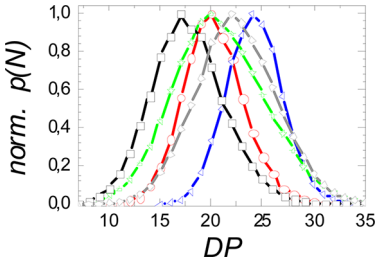


**Figure 1.** Normalized probability distributions $p(N)$ as a function of the degree of polymerization DP obtained from MALDI-ToF: black squares, **1**; gray diamonds, **2**; green stars, **3**; red circles, **3b**; blue triangles, **3a**.

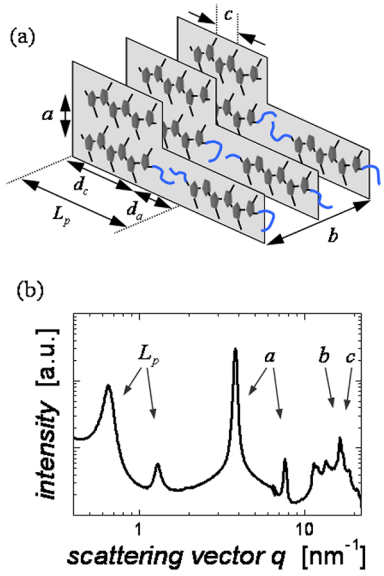


**Figure 2.** (a) Scheme of the semicrystalline structure of rrP3HT: $a$, $b$, and $c$ are the crystal lattice constants; $d_c$ and $d_a$ are the thicknesses of crystalline and amorphous layers, respectively; $L_P = d_c + d_a$ is the long period. (b) Combined (bulk) small- and wide-angle X-ray patterns of **3a**. The reflections resulting from the structures in (a) on the different length scales are indicated.

All samples were first investigated by differential scanning calorimetry (DSC; Figure 3). Several observations can be made: All samples exhibit three transitions including side-chain crystallization, which have been observed before for low molecular weight P3HT.[30]

While the highest temperature transition has been attributed to crystallization and melting of the backbone and the transition at ∼60 °C to alkyl side-chain ordering, complementary scattering experiments did not show structural changes that correspond to the DSC signal at 110 °C.[30] For the highest molecular weight sample, **3a**, the transition at 60 °C was visible,


dx.doi.org/10.1021/mz3003769 | ACS Macro Lett. 2012, 1, 1170−1175

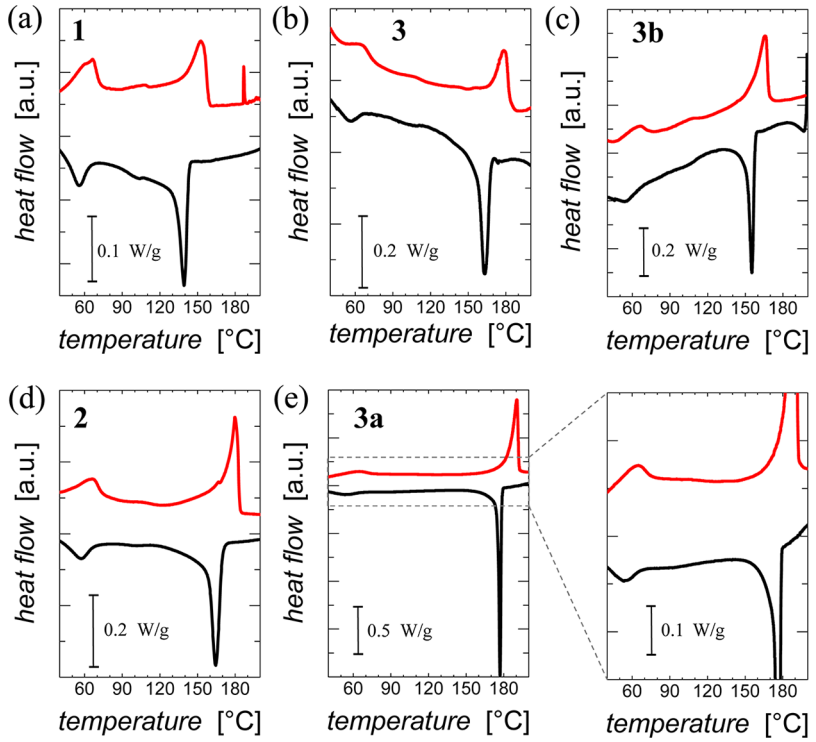


**Figure 3.** DSC cooling and heating traces of all samples at a rate of 10 K/min. Transition temperatures and enthalpies are summarized in Table 1. The spike at ~190 °C in (a) arises from noise of the instrument.

while the one at 110 °C was very weak. The crystallization and melting enthalpies for backbone melting were found to vary considerably up to a factor of ~3 among the samples, with a rough trend of larger enthalpies for higher DP (Table 1). Especially for the very low molecular weight samples, it is difficult to isolate the transition related to backbone melting from the lower temperature transitions (Figure 3a). For the narrowly distributed **3a** with DP = 24 and PDI = 1.06, a sharp high temperature transition was visible. The reliable integration of the cooling trace gave a $\Delta H_c$ = 29.2 J/g. The corresponding WAXS patterns were analyzed to investigate the origin of the rather large differences in the melting enthalpies in more detail.

WAXS on isotropic bulk samples after cooling from the melt can give qualitative information on the crystallinity of the samples. During cooling, a step profile consisting of alternating isothermal steps and cooling at 10 K/min was used resulting in an average cooling rate of 5 K/min (Figure S2). When this procedure was used, the scattering pattern did not change further by the end of each isothermal crystallization step. Figures S3a–d compare the WAXS patterns in the molten state (a, b) and at 40 °C (c, d) (two graphs are shown as WAXS patterns were recorded on different instruments with different resolution). As Figures S3c,d show, the WAXS intensities of different samples were very similar at 40 °C. This demonstrates that their degree of crystallinity was comparable, even though the DSC traces show large differences. The mixed index reflections at $q$ > 16 nm$^{-1}$ were visible for all samples, which demonstrated the ordered state of the side chains (Figure S3c,d).[30] An inspection of the temperature-dependent WAXS patterns is instructive to obtain information about the DSC transition at 110 °C. Figure S3e,f shows the WAXS patterns of the two narrowly distributed samples **3a** (e) and **3b** (f) at three temperatures. No mixed index reflections were visible for both samples at 130 °C (red squares) but were already present at 80 °C (gray triangles) and fully visible at 40 °C (open circles). Consistent with the literature, these reflections were better visible for **3b**, that is, the sample with a smaller DP.[30] A more detailed analysis of these reflections will be presented in a further publication, and the interested reader is directed to a comprehensive review by Brinkmann et al.[31] Here we note that, in contrast to previous reports, scattering experiments do indicate ordering of the alkyl side chains already at 110 °C, as seen by the appearance of mixed indices and also by the slight bump in the DSC heating curves. This finding is in agreement with results from Pascui et al. who observed that above 60 °C the side chains are less mobile than in the amorphous phase.[32]

The similar intensities of the WAXS reflections is seemingly in contradiction with the enthalpies of melting and crystallization obtained by DSC. To resolve this disagreement, the temperature-dependent behavior of the semicrystalline morphology of alternating crystalline and amorphous layers, reflected by the long period $L_p$ (see also Figure 2), was studied. As all investigated samples are 100% regioregular, we can exclude fractionation caused by the single distributed TT unit as present in conventionally, NidpppCl$_2$-polymerized rrP3HT.[29] Figure 4a shows the Lorentz-corrected SAXS patterns of **3a** (blue, DP = 24, PDI = 1.06) and **3b** (red, DP = 20, PDI = 1.06) together with the patterns of the corresponding as-synthesized sample **3** (green, DP = 21, PDI = 1.15) at 40 °C. All three samples clearly show first and second order $L_p$ peaks; **3a** even displays a third order reflection. It is interesting that the $L_p$ peak positions of **3** and **3a** coincide, although the DPs are 21 and 24, respectively. In contrast, the peak $L_p$s of **3** and **3b** are different but their DPs are 21 and 20, respectively. On the basis of the most probable chain length, **3** and **3b** should have similar values of $L_p$, as their peak molecular weights match well (compare red, green, and blue curves in Figures 1 and 4a). Hence, we conclude that, if fractionated


dx.doi.org/10.1021/mz3003769 | ACS Macro Lett. 2012, 1, 1170–1175

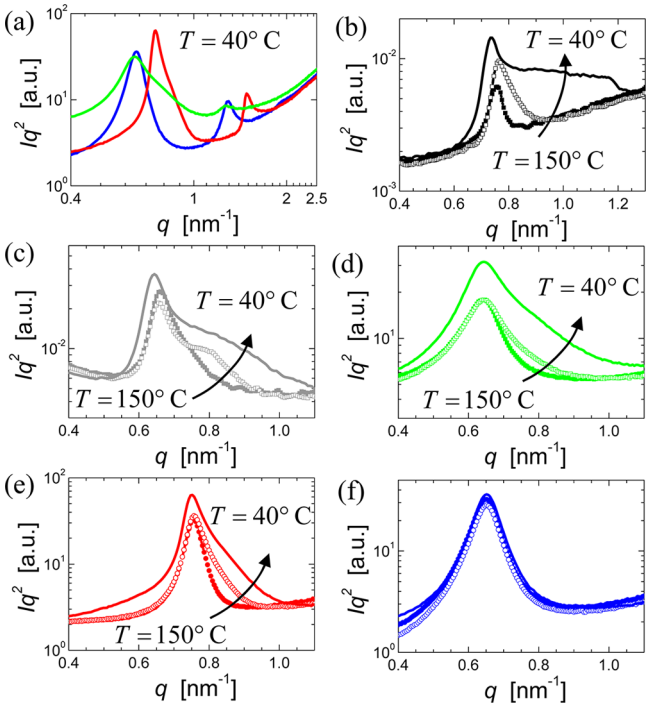


**Figure 4.** Lorentz-corrected SAXS patterns of dfP3HT: (a) Comparison of **3** (green), **3b** (red), and **3a** (blue) at 40 °C. Patterns of different samples at 150 °C (filled symbols), 130 °C (open symbols) and 40 °C (line): (b) **1**, (c) **2**, (d) **3**, (e) **3b**, and (f) **3a**. The samples were cooled using a step profile with isothermal steps. The patterns shown were taken at the end of each isothermal step.

crystallization occurs in chain-extended crystals, the $L_P$ is determined by the longest chains that crystallize first. This can also explain the observation that for low degrees of polymerization the $L_P$ is larger than the average contour length $l_c$ determined by MALDI-ToF.[30] This is further illustrated by comparing Figure 1 with $L_P$ and $l_c$ (Table 1): While $l_c$ is determined using the number average degree of polymerization according to $l_c = (DP - 1)/0.383$ nm, the peak maximum of $L_P$ is mostly set by the longest chains; hence, $L_P$ scales with the high molecular weight onset rather than with the DP.

However, the most striking observation in the SAXS patterns was changing peak shapes of $L_P$ during cooling. The same cooling program of alternating isothermal periods and 10 K/min cooling rates was applied. The scattering patterns shown here were all taken at the end of each isothermal step, where the scattering patterns remained invariant (Figure S2). All samples except **3a** developed shoulders at the high scattering vector side of the $L_P$ peak maximum, the extent of which varied with DP and PDI. This effect was strongest for sample **1** (DP = 18, PDI = 1.15, Figure 4b) and weakest for **3b** (DP = 20, PDI = 1.06, Figure 4e). The two samples **2** and **3** with similar DP and PDI showed a similar extent of FC (Figure 4c,d). Only the shape of the $L_P$ of **3a** (DP = 24, PDI = 1.06) remained invariant with decreasing temperature (Figure 4f).

From these results it becomes clear that samples **1**, **2**, **3**, and **3b** show fractionated crystallization (FC), that is, chains of different lengths crystallize at different temperatures. Qualitatively, the tendency to fractionate is more pronounced for larger polydispersities and smaller molecular weights, which is in accordance with the results of *n*-alkanes.[9] There, the effect of polydispersity was approximated by binary mixtures of monodisperse *n*-alkanes with varying difference in chain length. If the values of *n* were sufficiently similar, a "solid solution" was formed, that is, the chains of different length were incorporated into the same layers and a single layer-to-layer distance was observed that was intermediate of the pure components.[10] For binary mixtures with larger differences in chain length, for example, $n$ = 30 and 40, the chains fractionate, that is, chains of different length separate spatially, and two reflections corresponding to two different layer to layer distances were observed in electron diffraction.[10] Longer *n*-alkanes with *n* well above 100 are less prone to FC. Zeng et al. have studied binary mixtures of long alkanes with $n > 100$.[12,33,34] They found that the chains did not fractionate but instead formed a semicrystalline superstructure with the long chains protruding the crystalline layers on both sides. Although a quantitative comparison of FC in *n*-alkanes and dfP3HT is difficult, the results are qualitatively similar.

Note that we have also conducted the same set of experiments with well-defined, conventionally initiated rrP3HT exhibiting one single TT defect. The trends were less pronounced and not as consistent as the results of dfP3HT presented here (Figure S4, Figure S5, Table S1). Not surprisingly, the presence of a single TT unit has a large effect on the thermal properties for small degrees of polymerization.

The phenomenon of FC also provides an explanation why the melting enthalpies $\Delta H_m$ of **1**–**3** vary drastically (Table 1). The similar WAXS patterns suggest a similar degree of crystallinity in all samples (Figure S3). However, the samples exhibiting FC crystallize over a large temperature range, which exacerbates proper melting peak integration. These same samples also show a reduced melting enthalpy compared to **3a**, in which FC is absent (Table 1). Hence, the apparent reduction of crystallinity in samples **1**, **2**, **3**, and **3b** arises at least partially from the inability to integrate the entire area under the curve where main-chain melting occurs. This is additionally complicated by overlapping of main-chain crystallization with alkyl chain ordering, which sets in at 110° (Figure 3a).

Due to the absence of FC for the used cooling rate, the DSC melting and crystallization peak of **3a** is narrow and well above the temperatures at which the side chains start to order (Figure 3e). In all other samples, side chain ordering is accompanied by further main-chain crystallization arising from FC. In samples with sufficiently high molecular weights where FC is more likely to be absent, side chain crystallization is kinetically hindered.[30] Hence, the observation of rapid side-chain crystallization *and* the separation of main-chain and chain-side crystallization of **3a** is ideal to study temperature-dependent changes of the (100)-WAXS reflection and the long period $L_P$ caused by ordering of the side chains. Figure 5a shows the $L_P$ peak of **3a** at four different temperatures between 150 and 40 °C. Figure 5b shows the integrated peak intensity as a function of temperature during cooling. From 180 to 150 °C, the intensity increases as the sample crystallizes in this temperature range (Figure 3e). Below 150 °C the intensity decreases with temperature, as the SAXS signal is related to the difference in average electron density between the crystalline and the amorphous layers. Because the thermal expansion coefficient of amorphous regions is higher compared to the crystalline domains,[35] a decrease in scattering contrast results upon cooling to ~110 °C.

At ~100 °C, that is, the temperature at which the side chains start to order, the integrated intensity of the $L_P$ increases again. The crystallization of the side chains leads to a densification of


dx.doi.org/10.1021/mz3003769 | ACS Macro Lett. 2012, 1, 1170–1175

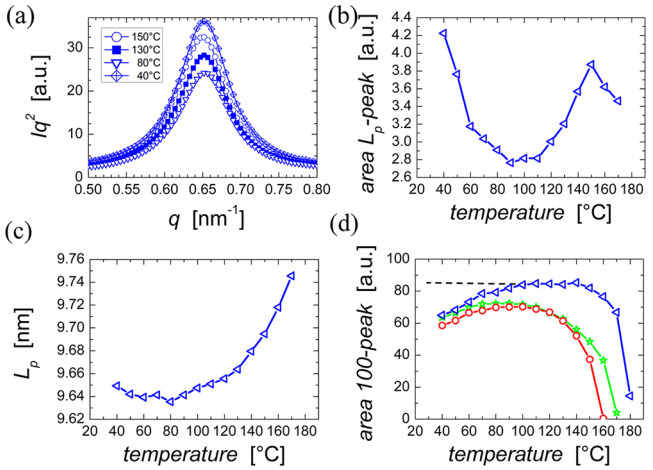


**Figure 5.** (a) Lorentz-corrected SAXS patterns of **3a** showing the first order $L_p$-peak at four different temperatures between 150 and 40 °C. (b) Temperature-dependent integrated $L_p$-peak intensity. (c) Temperature-dependent position of $L_p$. (d) Temperature-dependent integrated (100)-intensity of **3a** (blue triangles), **3b** (red circles), and **3** (green stars).

the alkyl layers within the crystal layers, thereby increasing their average electron density and, thus, the scattering contrast. Hence, side-chain ordering can also be observed by SAXS if the material crystallizes in a very narrow temperature range, and if this process is pure and not overlaid by other effects. In Figure 5c the position of $L_p$ as a function of temperature is shown. The decrease in $L_p$ with decreasing temperature can again be explained by the difference in the thermal expansion coefficients of amorphous and crystalline regions. The crystallization of the side chains does not play a role, because this process does not cause a difference in the thickness of the crystallites.

The integrated peak intensity of the (100)-WAXS peak is often used to characterize the crystallinity of rrP3HT. Figure 5d shows the evolution of the integrated intensity of the (100) reflection for **3a**, in which FC is absent, and for **3b** and **3** both of which show FC. Between 180 and 150 °C, the peak area of **3a** first increases as the sample crystallizes, remains constant down to 100 °C, and then decreases again below 100 °C. The same arguments used for the discussion of the temperature-dependent behavior of $L_p$ also apply here: side chain ordering increases the density of the alkyl layers. As a result, the electron density contrast between main chain (backbone) and side chain layers decreases, which is mirrored by the integrated (100)-peak intensity. For **3b** and **3** showing FC the temperature variation of the integrated (100) intensity differ, even though the curves are very similar at 40 °C, indicating a similar degree of crystallinity (Figure S3). At higher temperatures the integrated intensities are always below those of **3a**. Thus, for **3b** and **3** the effects of ongoing main chain crystallization and side chain ordering overlap and cancel. This result shows that care has to be taken when using integrated (100) intensities to obtain information about main-chain crystallinity, as alkyl-chain crystallization also influences the (100)-WAXS reflection.

What remains open here is the dependence of FC on the cooling rate. While the herein used step temperature program with an average cooling rate of 5 K/min allows for the observation of FC in samples **1**, **2**, and **3b**, sample **3a** with the highest molecular weight and the lowest polydispersity does not show FC. However, a fractionation process of **3a** might be observed if isothermal experiments are used in which the crystallization temperature is chosen such that the size of thermodynamically stable lamellae corresponds to a chain length that is within the distribution of **3a**.[29] To further study the phase behavior of polydisperse P3HT chains, it might be more straightforward to use monodisperse molecules of different lengths, which can be blended in a controlled way, similar to what has been done with *n*-alkanes.[9] The materials used here were prepared by preparative GPC, hence, it seems highly challenging to reproduce exactly the same chain length distributions, and batch-to-batch variations are likely.

We conclude that in low molecular weight defect-free P3HT samples even with very low PDI longer chains crystallize first into lamellar stacks during cooling from the melt, whereby shorter chains are being rejected from the growth front. These shorter chains only crystallize at lower temperatures when thinner lamellae become thermodynamically stable. While the herein used temperature program shows FC to be more prevalent for lower molecular weights and larger polydispersities, this mechanism of fractionated crystallization should be valid for larger molecular weights as well. Because fractionated crystallization provides a mechanism by which all chains can crystallize, polydispersity does not largely influence the degree of crystallinity of samples **1**−**3** at room temperature. The ability of shorter chains to crystallize at later times within a preformed network of crystallites of longer chains highlights the intriguing question of the influence of boundary structure and amorphous regions between crystallites on charge carrier mobility.[13,14,19,22,23]

## ■ ASSOCIATED CONTENT

### Supporting Information

Additional analytical details. This material is available free of charge via the Internet at http://pubs.acs.org.

## ■ AUTHOR INFORMATION

### Corresponding Author

*E-mail: michael.sommer@makro.uni-freiburg.de.

### Present Address

[§]Makromolekulare Chemie, Universität Freiburg, Stefan-Meier-Straße 31, 79100 Freiburg, Germany.

### Notes

The authors declare no competing financial interest.

## ■ ACKNOWLEDGMENTS

P. K. and U.S. acknowledge the European Comission (NMP4-SL20010-246123) for funding. M.S. acknowledges funding from the EPSRC. The ESRF Grenoble and M. Sztucki are greatly acknowledged for the provision of synchrotron radiation facilities and assistance (beamline ID02). This work was carried out with support of the Diamond Light Source beamline in Oxford. The authors thank G. Reiter, T. Thurn-Albrecht and B. Lotz for fruitful discussions.

## ■ REFERENCES

(1) Strobl, G. *The Physics of Polymers*, 3rd ed.; Springer: Berlin and Heidelberg, Germany, 2007.

(2) Brinkmann, M. *J. Polym. Sci., Part B: Polym. Phys.* **2011**, *49*, 1218.

(3) Heeney, M.; McCulloch, I. Flexible Electronics: Materials and Applications. In *Electronic Materials: Science and Technology*; Wong, W. S., Salleo, A., Eds.; Springer: New York, 2009; pp 261−296.

(4) Hugger, S.; Thomann, R.; Heinzel, T.; Thurn-Albrecht, T. *Colloid Polym. Sci.* **2004**, *282*, 932.

(5) Salleo, A. *Mater. Today* **2007**, *10*, 38.
(6) Chang, J.-F.; Clark, J.; Zhao, N.; Sirringhaus, H.; Breiby, D. W.; Andreasen, J. W.; Nielsen, M. M.; Giles, M.; Heeney, M.; McCulloch, I. *Phys. Rev. B* **2006**, *74*, 115318/1−12.
(7) Dang, M. T.; Hirsch, L.; Wantz, G. *Adv. Mater.* **2011**, *23*, 3597.
(8) Crossland, E.; Rhami, K.; Reiter, G.; Steiner, U.; Ludwigs, S. *Adv. Funct. Mater.* **2011**, *21*, 518.
(9) Ungar, G.; Zeng, X. B. *Chem. Rev.* **2001**, *101*, 4157.
(10) Dorset, D. L. *Macromolecules* **1986**, *19*, 2965.
(11) Dorset, D. L.; Snyder, R. G. *J. Phys. Chem. B* **1999**, *103*, 3282.
(12) Zeng, X. B.; Ungar, G. *Macromolecules* **2001**, *34*, 6945.
(13) Street, R. A.; Northrup, J. E.; Salleo, A. *Phys. Rev. B* **2005**, *71*, 165202.
(14) Boudouris, B. W.; Ho, V.; Jimison, L. H.; Toney, M. F.; Salleo, A.; Segalman, R. A. *Macromolecules* **2011**, *44*, 6653.
(15) Kline, J. R.; McGehee, M. D.; Kadnikova, E. N.; Liu, J.; Frechet, J. M. J. *Adv. Mater.* **2003**, *15*, 1519.
(16) Zen, A.; Pflaum, J.; Hirschmann, S.; Zhuang, W.; Jaiser, F.; Asawapirom, U.; Rabe, J. P.; Scherf, U.; Neher, D. *Adv. Funct. Mater.* **2004**, *14*, 757.
(17) Zhang, R.; Li, B.; Iovu, M. C.; Jeffries-EL, M.; Sauvé, G.; Cooper, J.; Jia, S.; Tristram-Nagle, S.; Smilgies, D. M.; Lambeth, N. D.; Kowalewski, T; McCullough, R. D. *J. Am. Chem. Soc.* **2006**, *128*, 3480.
(18) Kline, J. R.; McGehee, M. D.; Kadnikova, E. N.; Liu, J.; Frechet, J. M. J.; Toney, M. F. *Macromolecules* **2005**, *38*, 3312.
(19) Zen, A.; Saphiannikova, M.; Neher, D.; Grenzer, J.; Grigorian, S.; Pietsch, U.; Asawapirom, U.; Janietz, S.; Scherf, U.; Lieberwirth, I.; Wegner, G. *Macromolecules* **2006**, *39*, 2162.
(20) Zen, A.; Pflaum, J.; Hirschmann, S.; Zhuang, W.; Jaiser, F.; Asawapirom, U.; Rabe, J. P.; Scherf, U.; Neher, D. *Adv. Funct. Mater.* **2004**, *14*, 757.
(21) Brinkmann, M.; Rannou, P. *Adv. Funct. Mater.* **2007**, *17*, 101.
(22) Brinkmann, M.; Rannou, P. *Macromolecules* **2009**, *42*, 1125.
(23) Crossland, E.; Tremel, K.; Fischer, F.; Rahimi, K.; Reiter, G.; Steiner, U.; Ludwigs, S. *Adv. Mater.* **2012**, *24*, 839.
(24) Goh, C.; Kline, R. J.; McGehee, M. D.; Kadnikova, E. N.; Fréchet, J. M. J. *Appl. Phys. Lett.* **2005**, *86*, 122110.
(25) Ballantyne, A. M.; Chen, L.; Dane, J.; Hammant, T.; Braun, F. M.; Heeney, M.; Duffy, W.; McCulloch, I.; Bradley, D. D. C; Nelson, J. *Adv. Funct. Mater.* **2008**, *18*, 2373.
(26) Pingel, P.; Zen, A.; Abellón, R. D.; Grozema, F. C.; Siebbeles, L. D. A.; Neher, D. *Adv. Funct. Mater.* **2010**, *20*, 2286.
(27) Iovu, M. C.; Sheina, E. E.; Gil, R. R.; McCullough, R. D. *Macromolecules* **2005**, *38*, 8649.
(28) Miyakoshi, R.; Yokoyama, A.; Yokozawa, T. *J. Am. Chem. Soc.* **2005**, *127*, 17542.
(29) Kohn, P.; Huettner, S.; Komber, H.; Senkovskyy, V.; Tkachov, R.; Kiriy, A.; Friend, R. H.; Steiner, U.; Huck, W. T. S.; Sommer, J.-U.; Sommer, M. *J. Am. Chem. Soc.* **2012**, *134*, 4790.
(30) Wu, Z.; Petzold, A.; Henze, T.; Thurn-Albrecht, T.; Lohwasser, R. H.; Sommer, M.; Thelakkat, M. *Macromolecules* **2010**, *43*, 4646.
(31) Brinkmann, M. *J. Polym. Sci., Part B: Polym. Phys.* **2011**, *49*, 1218.
(32) Pascui, O. F.; Lohwasser, R.; Sommer, M.; Thelakkat, M.; Thurn-Albrecht, T.; Saalwächter, K. *Macromolecules* **2010**, *43*, 9401.
(33) Zeng, X. B.; Ungar, G. *Phys. Rev. Lett.* **2001**, *86*, 4875.
(34) Zeng, X. B.; Ungar, G.; Spells, S. J.; Brooks, G. M.; Farren, C.; Harden, A. *Phys. Rev. Lett.* **2003**, *90*, 155508.
(35) Schmidtke, J.; Strobl, G.; Thurn-Albrecht, T. *Macromolecules* **1997**, *30*, 5804.